Article

Quantitative Inhibitor Fingerprinting of Metalloproteases Using Small Molecule Microarrays

Mahesh Uttamchandani, Wei L. Lee, Jun Wang, and Shao Q. Yao

J. Am. Chem. Soc., **2007**, 129 (43), 13110-13117• DOI: 10.1021/ja073914v • Publication Date (Web): 04 October 2007

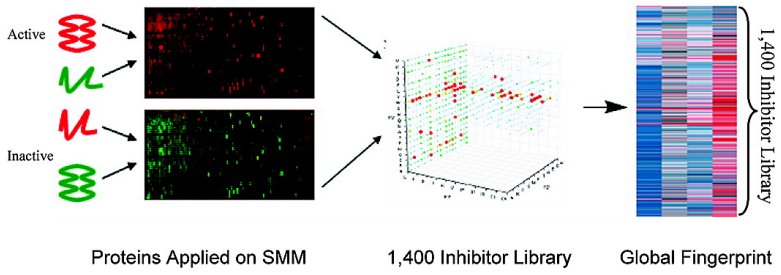

More About This Article

Additional resources and features associated with this article are available within the HTML version:

- Supporting Information
- Links to the 9 articles that cite this article, as of the time of this article download
- Access to high resolution figures
- Links to articles and content related to this article
- Copyright permission to reproduce figures and/or text from this article

View the Full Text HTML

J|A|C|S
ARTICLES
Published on Web 10/04/2007

Quantitative Inhibitor Fingerprinting of Metalloproteases Using Small Molecule Microarrays

Mahesh Uttamchandani,[†] Wei L. Lee,[†] Jun Wang,[‡] and Shao Q. Yao*[,†,‡,§]

Contribution from the Department of Biological Sciences, Department of Chemistry, and NUS MedChem Program of the Office of Life Sciences, 3 Science Drive 3, National University of Singapore, Singapore 117543

Received May 30, 2007; E-mail: chmyaosq@nus.edu.sg

Abstract: Current methods to identify interactions on small molecule microarrays (SMMs) introduce false positives that are difficult to dissect from the "real" binding events without tedious downstream re-evaluation. To specifically elucidate only activity-dependent ligand binding interactions, we have developed a technique that can be universally applied to present SMM systems. Our method makes use of a dual-color application strategy and is based on the simultaneous application of differentially treated samples. Overcoming the limitations of slide-to-slide variation, this method directly revealed activity-dependent interactions through a one-step application of protein samples on SMMs. Besides providing lead molecules for further development, the high-throughput screening results confer activity-dependent fingerprints for quantitative characterization and differentiation of proteins. The procedure was tested using a synthetic hydroxamate peptide library with 1400 discrete sequences permuted combinatorially across P_1', P_2', and P_3' positions. Functional profiling across a panel of metalloproteases provided 44 800 datapoints within just eight SMM slides. These data were globally analyzed for activities, specificity, potency, and hierarchical clustering providing unique insights into inhibitor design and preference within this group of enzymes. Quantitative K_D measurements performed on SMMs using one of the enzymes in the panel, Anthrax Lethal Factor, the toxic component of a notorious bioterror agent, unraveled several lead micromolar binders for further development. Overall, the effectiveness of the SMM platform is shown to be enhanced and extended using the strategy presented in this work.

Introduction

The challenge of large-scale, quantitative determination of protein−ligand interactions in high-throughput calls for the development of microarray-based platforms that offer rapid and cost-effective screening solutions.[1] One such promising technology is the small molecule microarray (SMM), where compounds are spatially addressed in high-density grids on planar glass substrates and simultaneously interrogated with suitable proteins and other targets.[1a] This offers a cheap and convenient method for the screening of thousands of compounds rapidly and has been successfully used in ligand identification,[2] and more recently in protein profiling.[3] The utility of SMMs as a routine platform for high-throughput discovery has however been limited, primarily because immobilized compounds first typically had to be decoded before they could be identified or high attrition rates prevented true binders from being immediately identified (due to nonspecific/false positive/functionally irrelevant binding), making them difficult to be used in protein fingerprinting experiments.[4]

Herein, we report a novel SMM platform that addresses these problems. By employing (1) a target-oriented library of individually synthesized compounds in which every member was characterized prior to spotting on the glass surface; (2) dual-color reciprocal protein labeling/screening strategy; and (3) simultaneous and quantitative measurements of multiple protein−ligand binding interactions, we were able to immediately and reliably elucidate the activity-dependent binding profiles of

[†] Department of Biological Sciences.
[‡] Department of Chemistry.
[§] NUS MedChem Program of the Office of Life Sciences.

(1) For representative reviews on various microarray-based platforms, see: (a) Duffner, J. L.; Clemons, P. A.; Koehler, A. N. *Curr. Opin. Chem. Biol.* **2007**, *11*, 74−82. (b) Tomizaki, K. Y.; Usui, K.; Mihara, H. *ChemBioChem* **2005**, *6*, 782−799. (c) Kung, L. A.; Snyder, M. *Nat. Rev. Mol. Cell. Biol.* **2006**, *7*, 617−622. (d) Shin, I.; Cho, J. W.; Boo, D. W. *Comb. Chem. High-Throughput Screening* **2004**, *7*, 565−574.

(2) (a) MacBeath, G.; Koehler, A. N.; Schreiber, S. L. *J. Am. Chem. Soc.* **1999**, *121*, 7967−7968. (b) Kuruvilla, F. G.; Shamji, A. F.; Sternson, S. M.; Hergenrother, P. J.; Schreiber, S. L. *Nature* **2002**, *416*, 653−657. (c) Barnes-Seeman, D.; Park, S. B.; Koehler, A. N.; Schreiber, S. L. *Angew. Chem., Int. Ed.* **2003**, *42*, 2376−2379. (d) Uttamchandani, M.; Walsh, D. P.; Khersonsky, S. M.; Huang, X.; Yao, S. Q.; Chang, Y. T. *J. Comb. Chem.* **2004**, *6*, 862−868. (e) Gosalia, D. N.; Diamond, S. L. *Proc. Natl. Acad. Sci. U.S.A.* **2003**, *100*, 8721−8726. (f) Bradner, J. E.; McPherson, O. M.; Mazitschek, R.; Barnes-Seeman, D.; Shen, J. P.; Dhaliwal, J.; Stevenson, K. E.; Duffner, J. L.; Park, S. B.; Neuberg, D. S.; Nghiem, P.; Schreiber, S. L.; Koehler, A. N. *Chem. Biol.* **2006**, *13*, 493−504. (g) Kanoh, N.; Kumashiro, S.; Simizu, S.; Kondoh, Y.; Hatakeyama, S.; Tashiro, H.; Osada, H. *Angew. Chem., Int. Ed.* **2003**, *42*, 5584−5587. (h) Kohn, M.; Wacker, R.; Peters, C.; Schroder, H.; Soulere, L.; Breinbauer, R.; Niemeyer, C. M.; Waldmann, H. *Angew. Chem., Int. Ed.* **2003**, *42*, 5830−5834. (i) Funeriu, D. P.; Eppinger, J.; Denizot, L.; Miyake, M.; Miyake, J. *Nat. Biotechnol.* **2005**, *23*, 622−627.

(3) (a) Takahashi, M.; Nokihara, K.; Mihara, H. *Chem. Biol.* **2003**, *10*, 53−60. (b) Reddy, M. M.; Kodadek, T. *Proc. Natl. Acad. Sci. U.S.A.* **2005**, *102*, 12672−12677.

(4) Sun, H.; Chattopadhaya, S.; Wang, J.; Yao, S. Q. *Anal. Bioanal. Chem.* **2006**, *386*, 416−426.

10.1021/ja073914v CCC: $37.00

proteins against immobilized chemical libraries *en masse*. A global analysis directly performed with the profiles provided valuable insights into protein characteristics, revealing activity-dependent protein fingerprints. For the present study, we selected different members of the metalloprotease family as our proteins of interest, as enzymes are among the most difficult (due to their delicate nature) yet valuable (due to their widespread involvement in biological processes) classes of proteins to study in a microarray format.[4] Metalloproteases, in particular, are a group of broad and diverse enzymes critically involved in the progression of a variety of diseases and bear important roles in metabolism as well as intra- and extracellular physiology.[5] Modulating these proteins using small molecule therapeutics provides a potential handle for the effective management and treatment of diseases such as cancer and arthritis as well as combating infections from pathogens like botulinum and anthrax.[6] This report serves, to our knowledge, as the first large-scale quantitative application of protein fingerprinting on a small molecule array that enables the functional discrimination among closely related protein members, fueling opportunities in drug design and discovery.

Materials and Methods

Materials. All chemicals were purchased at the highest grade available from commercial vendors and used without further purification, unless otherwise noted. All reactions were carried out under an N_2 atmosphere with HPLC grade solvents, unless otherwise stated. ESI mass spectra were acquired in both the positive and negative mode using a Finnigan/Mat TSQ7000 spectrometer. Analytical RP-HPLC separations were performed on a Phenomex C_{18} column (150 mm × 3.0 mm), using a Shimadzu Prominence HPLC system equipped with a Shimadzu SPD-20A detector. Eluents A (0.1% TFA/acetonitrile) and B (0.1% TFA/water) were used as the mobile phases. Active enzymes were acquired commercially, specifically Anthrax LF and Thermolysin from Calbiochem (Merck, Germany) and Collagenase and Carboxypeptidase from Sigma-Aldrich (USA). Fluorogenic substrates were purchased from List Biological Laboratories (USA), Calbiochem (Merck, Germany), and Molecular Probes, Invitrogen (California).

High-Throughput Screening on SMMs. Protein samples were minimally labeled with Cy3 and Cy5 *N*-hydroxysuccinimide esters (Amersham, G.E. Healthcare, USA) for 30 min on ice. The unreacted esters were quenched with a 10-fold molar excess of hydroxylamine or using 5 mM Tris (pH 8.0), for a further 15 min. Excess dye was further removed by size exclusion on a Sephadex G-25 column (Amersham, G.E. Healthcare, USA). The labeled proteins were confirmed to retain their native enzymatic activity by positive cleavage of their respective fluorogenic substrates. The designated inactive channel protein was first heat treated at 95 °C for 10 min and immediately cooled on ice. Enzymatic activity was confirmed to be lost by this procedure using activity assays with respective fluorogenic substrates. The heat-inactivated enzyme was then mixed with protein from the active channel and reconstituted in a final buffer volume of 100 μL PBS (pH 7.4) containing 1% bovine serum albumin (BSA). A total of approximately 8 μg of protein (4 μg in each channel) was applied under a coverslip to the arrays in this manner, and reciprocal experiments (with the designated dye channels inverted) were performed in parallel. The samples were incubated with the arrays in a humidified chamber for 2−4 h at room temperature, before repeated rinses with water, typically 2 × 2 min washes with gentle shaking. Excessive washing beyond 10 min was found to reduce correlations with microplate screening results. Slides were scanned using an ArrayWoRx microarray scanner installed with the relevant filters Cy3 - $\lambda_{ex/em}$ = 548/595 nm, Cy5 - $\lambda_{ex/em}$ = 633/685 nm. Optimization of procedures was first performed using thermolysin as a model before general adoption with the other enzymes.

K_D Analysis on SMMs. Using dose-dependent protein application on the arrays, we were able to extract K_D values against all of the positively binding small molecules simultaneously. A threshold was set to restrict analysis to only positive binders. A protein concentration series diluted across a 2-fold concentration range (from 4.8 μM to 150 nM for Thermolysin and from 2.4 μM to 75 nM for Anthrax LF) was applied on the microarrays in duplicate. The Cy3 channel was selected to designate the active channel for this experiment. The microarray data were extracted using the ArrayWoRx software and fitted using the following relationship, under the assumption that equilibrium is achieved during the incubation period:

$$\text{Observed fluorescence of } x = \frac{[\text{Maximum fluorescence, } x] \times [\text{Protein concentration}]}{K_D + \text{Protein concentration}}$$

Saturation dynamics observed when plotting *Observed fluorescence* against the applied *Protein concentration* were then fitted to the above equation using the Graphpad Prism software v.4.03 (GraphPad, San Diego, USA) revealing the binding dissociation constant, K_D, of the various positively identified small molecules. Only fits that correlated accurately with the experimental results ($r > 0.9$) were accepted.

IC_{50} Measurements. Concentration-dependent measurements were performed to confirm the potency of representative inhibitors within the library set. Inhibitors exhibiting a range of potencies for selected metalloproteases were identified from the microarray screens and evaluated using IC_{50} measurements. Briefly, dose-dependent reactions were performed by varying the concentrations of the inhibitor, under the same enzyme concentration. A 2-fold dilution series from approximately 25 μM to 390 nM (final reaction concentration) was prepared for each inhibitor in black 384-well plates. Substrates and enzymes for Anthrax LF were applied according to the following conditions: 0.2 pmol of the enzyme was combined with 2 nM MAPKKide substrate (List Biological Laboratories, USA) and inhibitor before being read at $\lambda_{ex/em}$ = 490/520 nm, with a cutoff at 515 nM. The 50 μL reaction was buffered in 20 mM Hepes (pH 7.4) supplemented with 0.1 mg/mL BSA and 0.01% Tween 20. Bodipy-FL-Casein (Molecular Probes, Invitrogen, USA) was used as the substrate for thermolysin and collagenase. Each 50 μL reaction was buffered in PBS (pH 7.4), with 1 μg of enzyme and 0.5 μg of substrate used per assay. The plates were allowed to incubate for 1 h at 37 °C before being interrogated for end-point fluorescence. The IC_{50} values were calculated by curve fitting against the concentration-dependent fluorescent plots using the Graphpad Prism software v.4.03 (GraphPad, San Diego, USA).

In Silico Docking Experiments. Molecular modeling was performed on an SGI IRIX 6.5 workstation using the SYBYL suite (version 7.2) installed with the FlexX docking software. Protein coordinates were retrieved from the Protein Data Bank; specifically inhibitor complexed crystal structures with the following accessions were employed: Anthrax LF: 1YQY. Structures of representative inhibitors were drawn using the "Sketch Molecule" option, and hydrogens were added. The biotin linker of the selected inhibitor was excluded to simplify the docking simulations. The structure was minimized using 100 iterations at 0.05 kcal/mol Å to relieve any torsional strain, and formal charges were assigned. The original protein structures were modified through the removal of water molecules. The docking sphere was set at 10 Å, centered at the zinc residue in the enzyme active site. Applying these criteria, the docking was performed for 30 iterations, with the most optimized configurations displayed. Proteins were displayed as either MOLCAD Connolly surfaces or ribbon diagrams.

(5) Turk, B. *Nat. Rev. Drug Discovery* **2006**, *5*, 785−799.
(6) (a) Tyndall, J. D. A.; Nall, T.; Fairlie, D. P. *Chem. Rev.* **2005**, *105*, 973−999. (b) Overall, C. M.; Kleifeld, O. *Nat. Rev. Cancer* **2006**, *6*, 227−239.

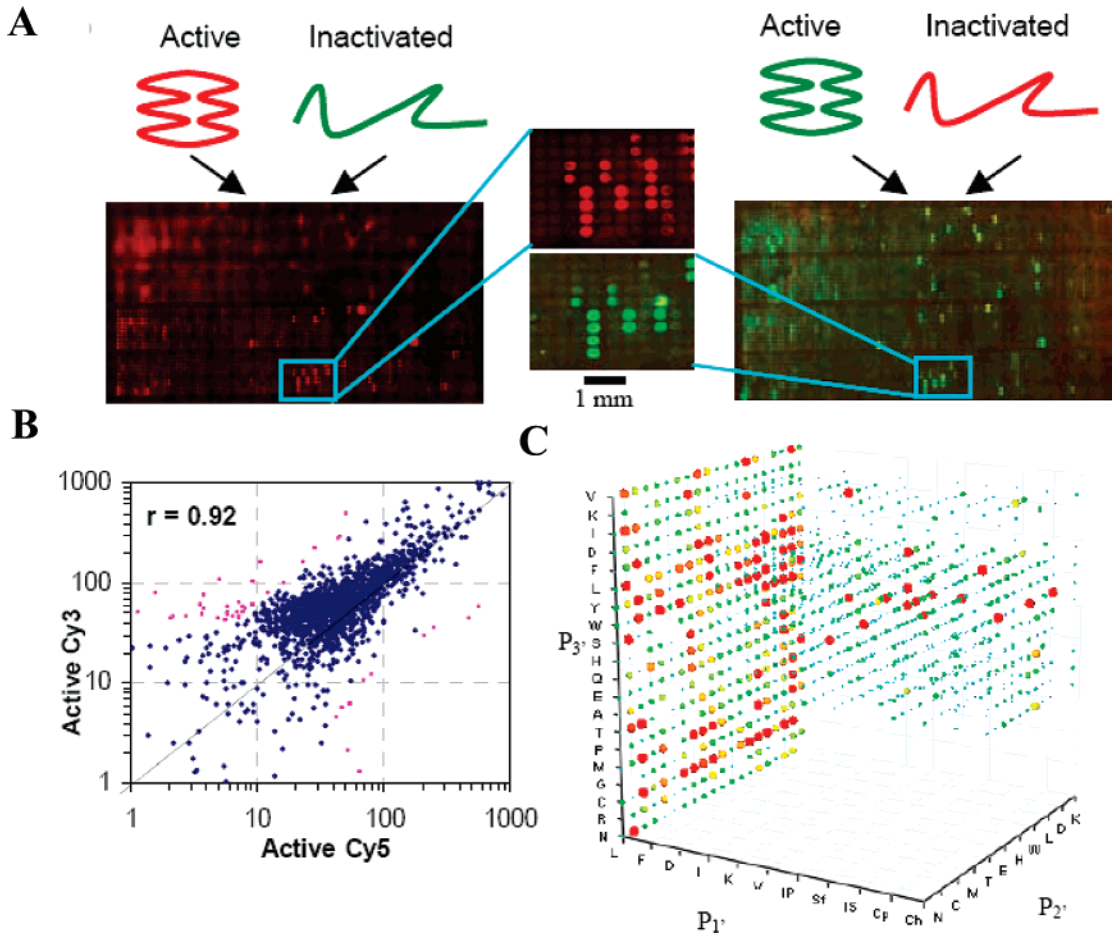

Figure 1. Dual-color reciprocal labeling/screening strategy. (A) Microarray images obtained with Thermolysin. The Cy3 channel is false colored in green, and the Cy5, in red. (B) Scatter plot of thermolysin results from reciprocal experiment. Data were filtered to remove aberrant points (indicated in pink). (C) Cube plot with 1400 inhibitors. Each inhibitor is represented by spheres plotted according to the P_1', P_2', and P_3' identities in the cube plot. Relative potency is indicated both by the color spectrum (cyan - least potent, red - most potent) and by the size of the sphere (small - least potent, big - most potent).

Scheme 1. Design of the 1400-Member Hydroxamate Small Molecule Inhibitor Library[a]

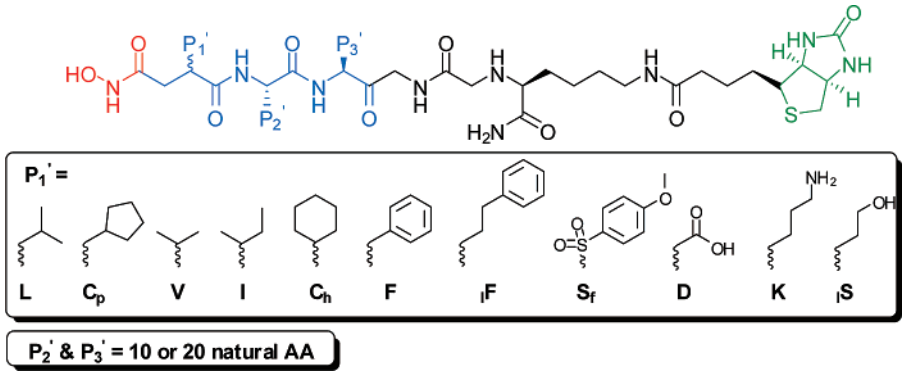

[a] The P_1', P_2', and P_3' positions in the inhibitor sequence were based on the standard protease nomenclature.

Results

SMM Design That Targets Metalloproteases. We identified various metalloproteases with representations from human pathogens, nonhuman sources, and bacterial origins, including thermolysin, collagenase, carboxypeptidase, and anthrax lethal factor (Table S1). We designed and synthesized a 1400-member small molecule inhibitor library that binds metalloproteases in an activity-dependent manner (Scheme 1 and Table S2); each compound features a potent hydroxamate zinc-binding group (red), a permutable specificity element for enzyme recognition (blue), a linker to extend the molecules from the slide surface (black), and a biotin anchor for site-specific immobilization on avidin-coated surfaces (green). Systematic permutation of both natural and unnatural amino acids across the P_1', P_2', and P_3' positions (key binding sites of most known metalloproteases) in the inhibitors provided a rich diversity of 1400 discrete and tractable sequences for protein fingerprinting. The chemical synthesis of the library was based on a previously optimized solid-phase approach (Scheme S1) by adopting the IRORI split-and-pool directed sorting technology.[7] This enabled the com-

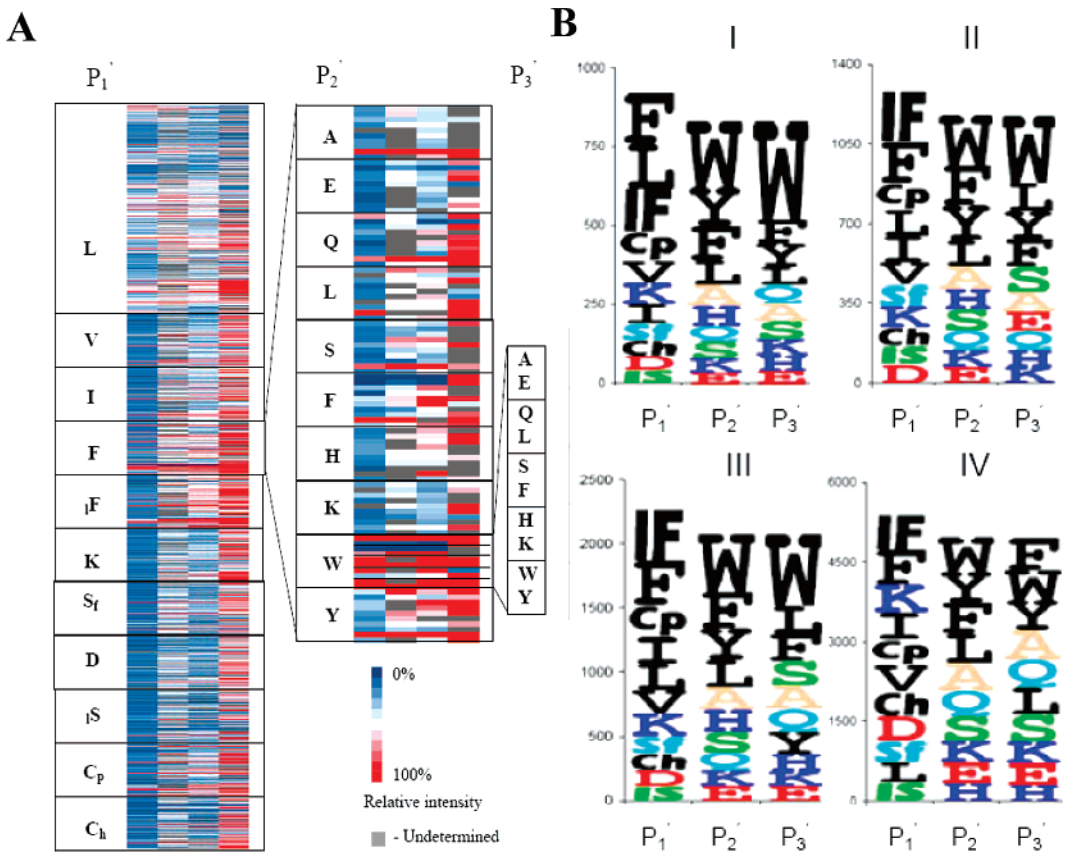

Figure 2. Activity-dependent fingerprints of (I) Thermolysin, (II) Collagenase, (III) Carboxypeptidase, and (IV) Anthrax LF with the 1400 molecule hydroxamate inhibitor library. (A) Colored heat maps displaying intensities with each of the inhibitors (scale inset). Inhibitors are sorted by $P_1' > P_2' > P_3'$ according to the order shown inset (labeled with single letter amino acid codes). The zoomed heat map shows inhibitor potencies of the sublibrary presenting **F** in the P_1' position. (B) Position specific scoring matrix (PSSM) representing averaged contributions to potency across P_1', P_2', and P_3' position. The height of each letter represents the weighted contribution of that residue to overall inhibitor potency. The side chains are colored according to their properties: hydrophobic/aromatic (black), acidic (red), basic (blue), polar (cyan), hydrophilic (green), and small (beige). The data are also presented as bar graphs in the Supporting Information (Figure S6).

binatorial synthesis of the entire library within three rounds of synthesis and sorting. Preparation of the library has been previously described.[7a,d] Randomly selected products were positively confirmed by LCMS and shown to be of sufficient purity.[7d] Taken together, our design features systematic comparisons across pure scaffolds, circumventing limitations of screening resolution and accuracy when using mixture-based libraries.[8] The library was subsequently spotted on an avidin-coated glass slide to generate the corresponding metalloprotease-targeting small molecule microarray in which the identity of every spot was known *a priori*.

Inhibitor Fingerprinting with Thermolysin on SMMs. To minimize false positives and ensure most data generated in SMM can be used directly for protein fingerprinting, we developed a dual-color reciprocal labeling/screening strategy, in which both the active and denatured forms of a target protein (e.g., thermolysin) were minimally labeled with two spectrally distinct dyes (Cy3 and Cy5) reciprocally and applied simultaneously to the same SMM (Figure 1 and Figure S1). This provides a dual-channel screening strategy in which one channel (containing denatured protein) is used as an internal control for direct and immediate elimination of nonspecific binding effects from the positive channel (containing active protein). By inverting the active/control channels, dye bias (from protein labeling) is further eliminated ensuring that the profiles generated are both activity-dependent and highly reliable.

High-quality and reproducible results were obtained, as shown in Figure 1 for thermolysin. Routinely, strong correlations were obtained between duplicate spots on the same slide ($r > 0.98$) and across independent slides ($r > 0.96$). After optimization of the screening protocols, we were able to eliminate most of the false binding signals in the heat-inactivation channel on the slide, confirming that the spot patterns observed were due to protein activity (Figure 1A). The intensity values arising from equal quantities of Cy3 and Cy5 dyes were determined to be equivalent on our scanning systems (Figure S2), enabling direct averaging and combination of the data obtained from both channels without the need for scaling or normalization. Across reciprocal channels, data correlation in general was high ($r = 0.92$), with a few points (<5% of the data) reproduced poorly. They were treated as artifacts and removed (indicated in pink Figure 1B). Averaged results from reciprocal experiments for the 1400-member library were visualized as a cube plot in Figure 1C. In order to correlate results obtained on the SMM platform with those from traditional systems, we performed solution-

(7) (a) Wang, J.; Uttamchandani, M.; Sun, L. P.; Yao, S. Q. *Chem. Comm.* **2005**, *7*, 717−719. (b) Wang, J.; Uttamchandani, M.; Li, J.; Hu, M.; Yao, S. Q. *Org. Lett.* **2006**, *8*, 3821−3824. (c) Wang, J.; Uttamchandani, M.; Li, J.; Hu, M.; Yao, S. Q. *Chem. Comm.* **2006**, 3783−3785. (d) Uttamchandani, M.; Wang, J.; Li, J.; Hu, M.; Sun, H.; Chen, K. Y.-T.; Liu, K.; Yao, S. Q. *J. Am. Chem. Soc.* **2007**, *129*, 7848−7858. (e) Leeuwenburgh, M. A.; Guerink, P. P.; Klein, T.; Kauffman, H. F.; van der Marel, G. A.; Bischoff, R.; Overkleeft, H. S. *Org. Lett.* **2006**, *8*, 1705−1708.

(8) Walsh, D. P.; Chang, Y. T. *Chem. Rev.* **2006**, *106*, 2476−2530.

Table 1. Motif Selectivity Comparisons[a]

Enzyme	Position			Reference
	P_1'	P_2'	P_3'	
Thermolysin	L, F, I	L, A, V, Y,	C, V, R, Y	[10]
	F, **L**, $_l$F, C_p	W, **Y**, F, **L**	W, F, **Y**, L	Present study
Anthrax LF	Y, L, I, M	P, Q, R, K	N, M	[11]
	F, I, A, L	T, Q, L, P	L, F, S, T	[10]
	$_l$F, **F**, K, **I**	W, Y, F, **L**	**F**, W, Y, A	Present study
Carboxypeptidase	F, W, L, V	N.A.	N.A.	[10]
	F, $_l$F , C_p, I	W, F, Y, L	W, F, L, S	Present study
Collagenase	L, G	P, V, T	L, T, A	[10]
	$_l$F, F, C_p, **L**	W, F, Y, L	W, F, Y, **L**	Present study

[a] The inhibitor selectivity exhibited from this study were tabulated with known substrate preferences for each metalloprotease (from both peptide-based and protein-based substrate motifs). This highlights the general similarities observed, with subtle differences when comparing substrate profiles and inhibitor profiles. Single-letter amino acid codes are used to denote all the preferred residues. The top four most potent residues are displayed from each study. The top four from the averaged profiles are shown for the present study and displayed in bold if also observed to be preferred in substrate sequences.

phase screening of the 400-member P_1' **L** sublibrary in microtitre-plate format. Despite fundamental differences between the solution-phase (in a microplate) and chip-based screening (in a microarray), we observed mostly consistent profiles from both platforms (Figure S4). This further confirmed the activity-dependence of the profiles obtained using SMMs, thus validating its potential for rapid differentiation of potency across closely related inhibitors.

Inhibitor Fingerprinting with Enzyme Panel on SMMs. Having optimized the platform and tested its capability, we went on to characterize various other metalloproteases. Using the same dual-channel screening approach, we applied these enzymes in reciprocal channels on the 1400-member hydroxamate SMM. Each enzyme was profiled as earlier described with thermolysin, using data from reciprocally duplicated experiments. This represented 11 200 independent data points on the SMMs that were processed for each enzyme (2 Microarray Slides × 1400 Inhibitors × 2 Duplicated Spots × 2 Channels) and distilled into the final fingerprint representing the 1400 inhibitors. The analysis further enabled false positive or nonspecific binders to be removed from the analysis through the subtraction of the inactive channel. The final activity-dependent fingerprints for four different metalloproteases are shown as colored heat maps in Figure 2A (and as cube plots in Figure S5). Data that were highly discordant between the reciprocal experiments were excluded, as described earlier (shown in gray in Figure 2A). The presence of 20 mM EDTA (a metal-chelating general metalloprotease inhibitor) was also shown to abolish the binding patterns with all the metalloproteases tested. This confirmed that the fingerprints obtained reflected the binding profiles of enzymes only in their truly functional state.

Each enzyme displayed characteristic patterns (Figure 2A). The P_1' **L** side chain, together with **F** and $_l$**F**, contributed highly to inhibitor potency. The P_1' position is generally regarded as the most important in governing selectivity of either substrates or inhibitors among metalloproteases.[6] Closer analysis with thermolysin further revealed a preference for **F**/**W** in the P_2' position and **W** in the P_3' position (Figure 1C and Figure 2A). In order to better visualize the differences across enzymes, the P_1' **F** sublibrary was magnified in Figure 2A. This highlighted that variations across the P_2' and P_3' positions also contributed significantly to binding intensity. This analysis revealed that aromatic residues **W**, **Y**, and **F** in the P_2' and P_3' positions were greatly favored by almost all the enzymes screened. Interestingly, almost irrespective of the P_2' side chain, **W** at the P_3' position was found to have a governing importance in inhibitor potency. The presentation of small hydrophobic side chains in the P_1' position and larger aromatics in the other prime pockets was encouraging as it agrees well with known potent metalloproteases inhibitors including GM6001, Batimastat, and Marimastat which also present **L** at the P_1' and **F** or **W** at the P_2' position in their scaffolds (Figure S3). Anthrax LF was the most promiscuous metalloprotease in the panel that displayed significant affinity with a considerable proportion of the library, warranting further investigation (*vide infra*). Aside from the relatively weakly associating $_l$**S** and $\mathbf{S_f}$ P_1' side chains, there was significant binding (as indicated with varying intensities of red) with many of the other P_1' side-chain categories (Figure 2A). The heat-map representation further enables direct comparisons and easy identification of either generic or selective inhibitors.

Average Inhibitor Fingerprints. Intensity values for all enzymes were thereafter averaged for each P_1', P_2', and P_3' position to globally visualize contributions to potency across the library. The results of this analysis were displayed both as position specific scoring matrixes (Figure 2B) and as bar graphs (Figure S6). Here we also confirmed earlier findings, where aromatic side chains were found to contribute strongly to inhibitor potency. The matrices highlighted that $_l$**F** and **F** consistently appeared among the top three side chains in the P_1' position for all four metalloproteases screened (Figure 2B). Additionally, across both P_2' and P_3' positions, it was observed that there was a large overall contribution from inhibitors bearing **W**. With peculiar clarity, it was further revealed that side chains classified as hydrophobic/aromatic contributed significantly to the overall potency of these inhibitors, as seen with the "black" residues occupying the uppermost positions in the matrices across all four enzymes. On the other hand, the charged and hydrophilic side chains occupied the lower-most portions of the matrices. This correlates very well with established findings against various metalloproteases, including those performed for

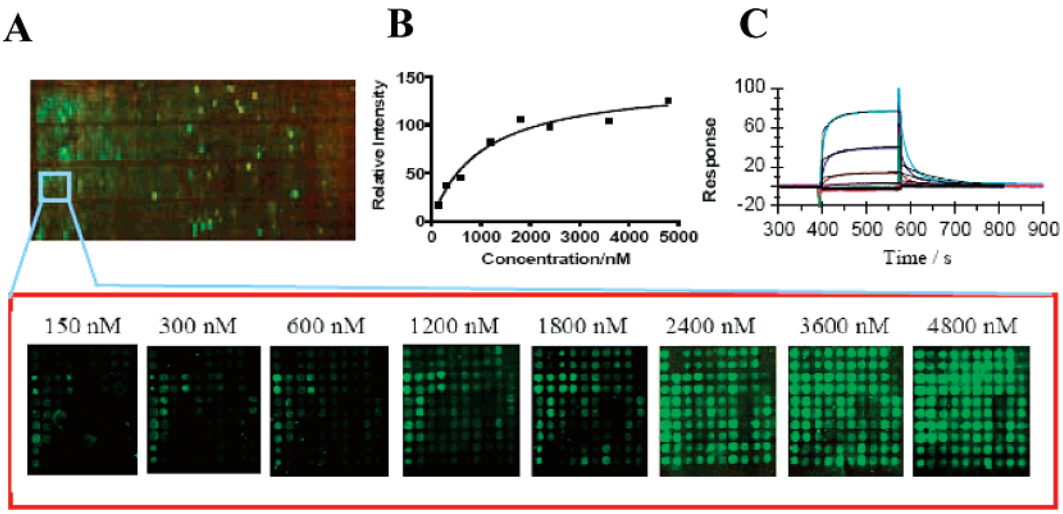

Figure 3. Large-scale K_D determination for thermolysin using SMMs. (A) Eight different concentrations of protein (only shown in the magnified region) were applied to the arrays. (B) The K_D response curve from duplicated microarrays with **L-A-R**. (C) Fitted SPR results with **L-A-R**.

Table 2. Comparison of K_D Values Obtained from the SMM and SPR Experiments against Thermolysin for Three Selected Inhibitors

inhibitor P_1'-P_2'-P_3'	K_D using SPR/μM	K_D using SMM/μM
L-A-R	1.55	1.02
L-I-W	1.49	2.05
L-L-C	1.44	2.14

the enzymes included in the panel.[6a] A detailed comparison is shown (Table 1). It is relevant to note that the best inhibitor scaffolds are identified by potent dissociation constants, while the best substrates are those that, in addition, provide good conversion and thus reversibility of binding.[9] Our analysis revealed that apart from the conserved residues that have been previously identified in putative substrate based screens, various side chains (including the unnatural side chains, $\mathbf{C_p}$ and $_\mathbf{l}\mathbf{F}$) have positive contributions toward inhibitor potencies. This new information may be used for future inhibitor design and improved efficacy across this class of proteins.

Top-100 Analysis. In order to delineate inhibitor selectivity across the panel of metalloproteases screened, we picked the top-100 inhibitors within each enzyme and used Venn diagrams to evaluate the distribution of these hits across the four-member metalloprotease panel (Figure S7). Combining samples of the top-100 hits from all four enzymes provided a set of 260 unique inhibitor sequences (Table S3). We also uncovered inhibitors that exhibited potency against two or more metalloproteases screened. This included three inhibitors that were potent against all four of the metalloproteases screened (Table S4).

Cluster Analysis. Hierarchical clustering was performed to group metalloproteases on the basis of the activity-dependent fingerprint results obtained. The alignments of the primary sequences of the metalloproteases used were presented in Figure S8. The enzyme panel was successfully clustered using the inhibitor fingerprints obtained against the 1400 inhibitors to produce a cladogram (Figure S9). As expected, Anthrax LF was revealed to be the most distinct in its inhibitor fingerprint. Carboxypeptidase and thermolysin formed a sister pair, highlighting the similarity in inhibitor preference between the two enzymes and across traditional clan groupings (Table S1). This inhibitor-based classification provides a useful way of looking at metalloproteases with functional relevance and can be used in future to profile inhibitor preference and selectivity within members of any given protein family.

Table 3. K_D and IC_{50} Results of Selected Inhibitors against Anthrax LF[a]

Inhibitor P_1' - P_2' – P_3'	K_D on SMM/μM	IC_{50}/μM
$_\mathbf{l}$**F-F-L**	0.81	2.0
F-W-L	0.71	2.2
I-Y-L	0.74	5.5
F-W-S	0.86	7.9
I-A-A	2.6	14.0
L-P-A	8.4	16.3
L-D-C	2.0	29.6
D-K-Q	5.6	>25
L-P-E	4.5	>25

[a] The inhibitors were grouped according to the IC_{50} results in different colors (high potency inhibitors in red, medium potency inhibitors in green, and weak inhibitors in blue).

***K_D* Determination with Themolysin on SMMs.** The ability to better enumerate the strength of binding interactions provides a useful window toward the convenient verification of potent inhibitors within huge chemical libraries.[12] In an effort to demonstrate this capacity on a large scale using SMMs, we first applied a range of concentrations of thermolysin with all the inhibitors simultaneously on the microarrays. The entire experi-

(9) Rishton, G. M. *Drug Discovery Today* **2003**, *8*, 86−96.
(10) (a) www.//merops.sanger.ac.uk. (b) Rawlings, N. D.; Morton, F. R.; Barrett, A. J. *Nucleic Acids Res.* **2006**, *34*, D270−D272.
(11) Turk, B. E.; Wong, T. Y.; Schwarzenbacher, R.; Jarrell, E. T.; Leppla, S. H.; Collier, R. J.; Liddington, R. C.; Cantley, L. C. *Nat. Struct. Mol. Biol.* **2004**, *11*, 60−66.
(12) (a) Stiffler, M. A.; Grantcharova, V. P.; Sevecka, M.; MacBeath, G. *J. Am. Chem. Soc.* **2006**, *128*, 5913−5922. (b) Gordus, A.; MacBeath, G. *J. Am. Chem. Soc.* **2006**, *128*, 13668−13669.

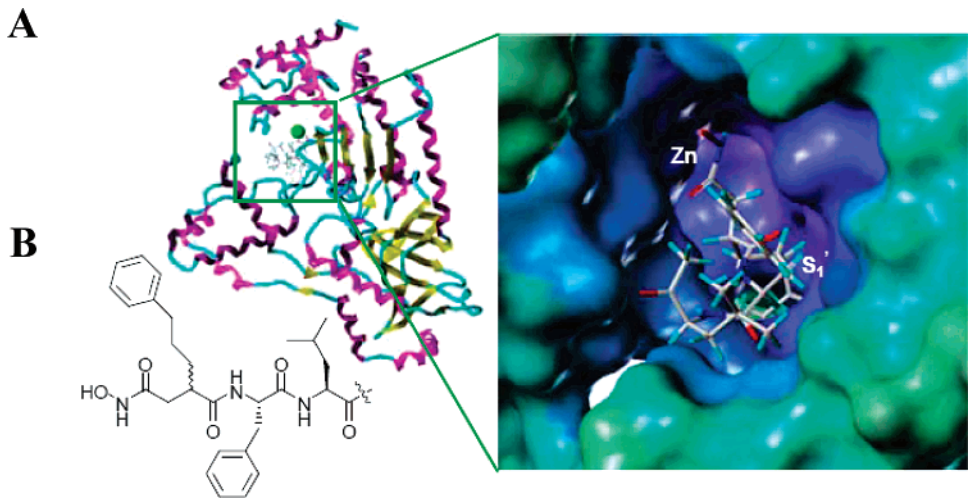

Figure 4. Docking configurations of **$_{I}$F-F-L** with Anthrax LF. (A) The zinc ion in the active site is shown as a green sphere in the ribbon diagram. The image is expanded to show the potential docking configuration in the enzyme active site. (B) Structure of **$_{I}$F-F-L**.

ment was performed in duplicate with 8 concentration points over 16 SMM slides as shown in Figure 3A. The data were fitted to a saturation dynamics relation, which assumes that when equilibrium is achieved, K_D information may be extracted from the resulting curves (Figure 3B). Upon subjecting the data to stringent filtering criteria (accurate curve fits ($r > 0.9$) and significant binding signals (above 50% relative intensity)), we were able to obtain the K_D for 43 inhibitors that showed a good affinity ($K_D < 4.8\ \mu M$) on the SMMs (Table S6). To confirm the accuracy of the values obtained, we picked three representative inhibitors for independent validation using surface plasmon resonance (SPR) (Figure 3C and Figure S10): results confirm that the K_D values obtained from the microarrays were highly consistent with those measured using SPR (Table 2), highlighting the utility of SMMs in quantitative binding experiments.

K_D Determination with Anthrax LF on SMMs. It has been an ongoing challenge to develop potent and selective inhibitors to treat the intoxication of anthrax, in tandem with established antibiotic therapies available.[13] Various groups have reported low micromolar inhibitors uncovered using various chemical approaches.[14] The most potent known inhibitor for Anthrax LF is a low nanomolar hydroxamate-based 14-mer peptide inhibitor that also strongly inhibits the serine protease furin.[15] With the aim of identifying potent/selective inhibitors that target Anthrax LF, we applied the enzyme in a concentration-dependent manner on the SMM to rapidly obtain K_D data for our library of inhibitors. As earlier described, 16 printed hydroxamate microarrays were used in duplicated experiments. Using similar stringent fitting and intensity criteria, we successfully obtained K_D values for 85 inhibitors within the dataset (Tables S5 and S7). We went on to select several promising inhibitors across various grades of potency for further evaluation. IC_{50} measurements were performed for a panel of nine inhibitors in solution-phase microplate experiments (Table 3 and Figure S11), which once again were shown to be highly correlated to the microarray-based results. Of significant interest, one of the inhibitors identified, **$_{I}$F-F-L**, was found to be selective for Anthrax LF across the panel of enzymes screened in the top-100 analysis. This inhibitor provided a potent K_D of 0.81 μM on the microarray and an IC_{50} of 2.0 μM. Several other inhibitors were also identified, including **F-W-L** and **I-Y-L** which were confirmed to exhibit strong binding potencies with Anthrax LF (Table 3).

Docked Position of Selected Inhibitor. The identified inhibitor, **$_{I}$F-F-L**, was also employed for docking analysis with Anthrax LF. As would be expected, the optimized docking configuration of the inhibitor/enzyme complexes revealed the inhibitor adopted an extended conformation, comfortably fitting along the substrate binding groove in the enzyme active site (Figure 4). The hydroxamate group from the inhibitor was observed to chelate to the bound zinc atom, while the P_1' side chain fitted deeply into the S_1' pocket. It was further observed that the P_2' and P_3' positions of the inhibitor contribute to the overall inhibition potency through the formation of hydrogen bonds and van der Waals interactions with the protein. Docking was also attempted with **F-W-L** and **I-Y-L**; however these inhibitors failed to dock appropriately with Anthrax LF. The reason for this is being investigated.

Discussion

The daunting task of screening huge chemical libraries has been ameliorated with the emergence of SMMs. There have however been limited examples exploiting this platform in a global manner for the elucidation of physiologically relevant interactions. We herein introduce a method that enables practitioners to rapidly hone in on biologically relevant hits using SMMs. High-throughput screens performed using a focused library of small molecule-based hydroxamate inhibitors revealed reproducible, unique, and informative signatures for each enzyme tested. The platform also facilitated the discovery of inhibitors with low micromolar potencies against thermolysin and anthrax lethal factors from *Bacillus anthracis* (a potential bioterror agent). Establishing functional differences through selective protein fingerprints using SMMs will not only enhance the understanding of proteins in biological systems but also further accelerate the discovery of efficacious therapeutic leads.

(13) (a) Moayeri, M.; Leppla, S. H. *Curr. Opin. Microbiol.* **2004**, *7*, 19−24. (b) Montecuccco, C.; Tonello, F.; Zanotti, G. *Trends Biochem. Sci.* **2004**, *29*, 282−285.
(14) (a) Panchal, R. G., et al. *Nat. Struct. Mol. Biol.* **2004**, *11*, 67−72. (b) Numa, M. M. D.; Lee, L. V.; Hsu, C.-C; Bower, K. E.; Wong, C.-H. *ChemBioChem* **2005**, *6*, 1−5. (c) Min, D.-H.; Tang, W.-J.; Mrksich, M. *Nat. Biotechnol.* **2004**, *22*, 717−723.
(15) Tonello, F.; Seveso, M.; Marin, O.; Mock, M.; Montecucco, C. *Nature* **2002**, *418*, 386.

Through our analysis, we uncovered several interesting results. Each metalloprotease provided a unique inhibitor fingerprint, with that for Anthrax LF being the most distinct. For nearly all the metalloproteases tested, there were several uniquely potent inhibitors uncovered (Figure 2). Consistent with previous findings,[10,11] we found that hydrophobic and aromatic side chains contribute greatly to inhibitor potency for all the enzymes tested. The most potent side chains included **L**, **$_l$F**, and **F** with aromatic side chains like **W**, **F**, and **Y** in the P_2' and P_3' positions across all four metalloproteases (Figure 2B). It was further demonstrated that by analyzing profiles of varied protein concentrations applied to the microarray, we were able obtain measurements of dissociation constants that were consistent with those independently performed on alternative platforms, like SPR. We followed through with the analysis of several of the potent inhibitors against Anthrax LF and discovered that the potencies were replicated with IC_{50} screens performed on a microplate. These revealed inhibitors such as **$_l$F-F-L** and **F-W-L** that had low micromolar potencies against Anthrax LF. Furthermore, it was uncovered that **$_l$F-F-L** was among one of the top-100 inhibitors and was further selective to only Anthrax LF within the panel of enzymes screened (Table S8). This makes it a promising candidate for further investigation and development.

Conclusion

In conclusion, the reciprocal dual-labeling strategy consumed minimal enzyme quantities and provided characteristic binding fingerprints for each enzyme tested. With the ability to independently manipulate proteins across each dye channel, potential false positives that contributed signals from the inactive channel were readily eliminated. Reciprocating the channels labeled over duplicate slides further enabled the removal of any dye bias, inherent systematic errors, or endogenous fluorescence from the analysis. This provided a conveniently implementable system for the elucidation of both reproducible and activity-dependent results from SMM studies. In traditional SMM studies, it is frequently only the best binders that are deconvoluted, leaving the majority of the dataset uncharacterized. With every member of the array known *a priori*, we were on the other hand able to extract a wealth of information through comprehensive analysis of the complete dataset and carried out protein fingerprinting on SMMs. We further demonstrated the first large-scale K_D determination for small molecule inhibitors using SMMs, highlighting its potential significance toward accelerating the discovery of potent molecules. Overall, our approach paves the way forward in microarray-driven research by capitalizing on the powerful capability and throughput offered from SMMs and providing useful tools for comprehensive proteomic evaluation and high-throughput screening applications in the future.

Acknowledgment. Funding support was provided by the National University of Singapore (NUS) and the Agency for Science, Technology and Research (A*STAR) of Singapore

Supporting Information Available: Scheme for library synthesis, complete protocols for array fabrication, K_D binding analysis, IC_{50} analysis, docking analysis, microarray controls, and additional images. This material is available free of charge via the Internet at http://pubs.acs.org.

JA073914V